Supplementary information

# Optimization of Low-Temperature Catalytic Cracking of Polyolefin Waste in Open-Batch Reactors Using Zeolite Beta with Controlled Intrinsic Properties

Hankyeul Kang[1], Junghwa Yoon[1], Dongwoo Jun[1], Ki Hyuk Kang[2], Insoo Ro[3], Soohwa Jeong[4], Jong Hun Kang[1,*]
[1]School of Chemical and Biological Engineering and Institute of Chemical Processes, Seoul National University, Seoul 08826, Republic of Korea
[2]Low-Carbon Petrochemical Research Center, Korea Research Institute of Chemical Technology (KRICT), Daejeon 34114, Republic of Korea
[3]Department of Chemical and Biomolecular Engineering, Seoul National University of Science and Technology, Seoul 01811, Republic of Korea
[4]Carbon Neutral Technology R&D Department, Korea Institute of Industrial Technology, Cheonan-si 31056, Republic of Korea
* E-mails: jonghunkang@snu.ac.kr

## Materials and Synthesis Information

### Commercial zeolite information

Commercial zeolites used in this work are as follows: ZSM-5 ($NH_4^+$-form, powder, $SiO_2$:$Al_2O_3$=23:1 nominal molar ratio, Thermo Scientific), Zeolite Y(1) (H-form, powder, $SiO_2$:$Al_2O_3$=30:1 nominal molar ratio, Alfa Aesar). Zeolite Y(2) (CBV712, $NH_4^+$-form, powder, $SiO_2$:$Al_2O_3$=12:1 nominal molar ratio, Zeolyst), and zeolite beta ($NH_4^+$-form, powder, $SiO_2$:$Al_2O_3$=25:1 nominal molar ratio, Alfa Aesar). All $NH_4^+$-form zeolites were converted to their H-form by calcining at 580 °C for 6 hours.

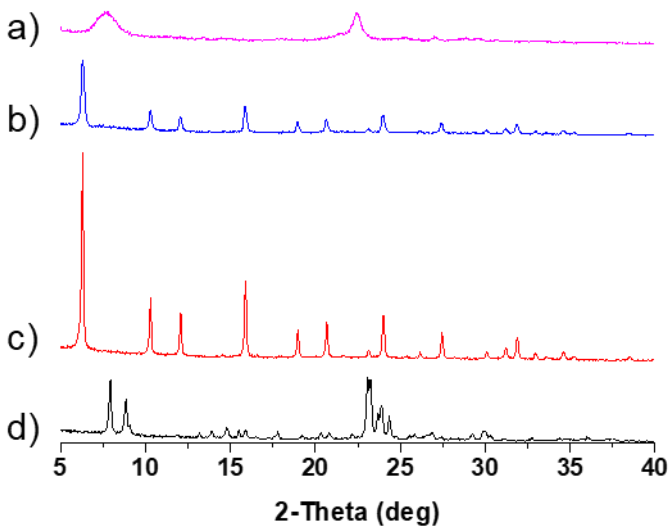


**Supplementary Figure 1. Powder X-ray diffraction profiles of commercial zeolites:** a) zeolite beta, b) zeolite Y(1), c) zeolite Y(2), d) ZSM-5

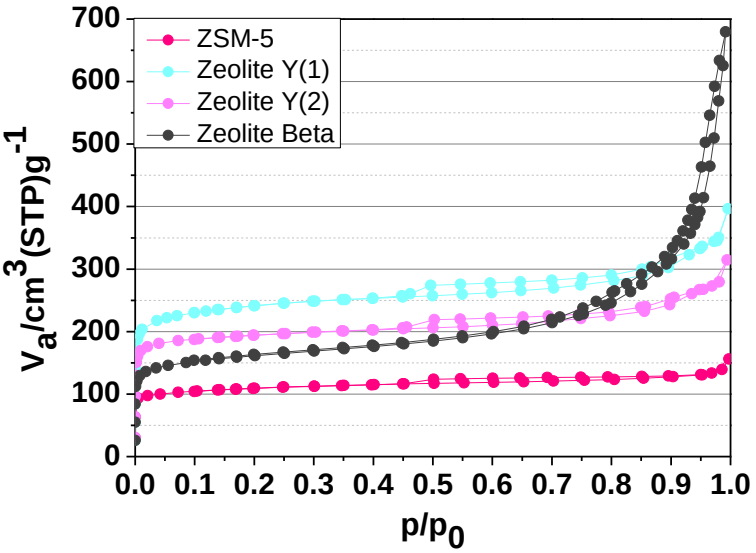


**Supplementary Figure 2. 77 K $N_2$ physisorption profiles of commercial zeolites**

**Supplementary Table 1. Physical properties of the commercial zeolites.**

| Sample | Crystal size (nm) | Si/Al† | $S_{BET}$ ($m^2/g$)‡ | $V_{mic}$ (cc/g)‡ | $S_{Ext}$ ($m^2/g$)‡ | $V_{meso}$ (cc/g)‡ |
|---|---|---|---|---|---|---|
| ZSM-5 | 100–1000 | 9.8 | 342 | 0.134 | 78 | 0.088 |
| Zeolite Y(1) | 100–1000 | 14.1 | 750 | 0.341 | 87 | 0.316 |
| Zeolite Y(2) | 100–1000 | 6.3 | 601 | 0.265 | 82 | 0.190 |
| Zeolite Beta | 10–100 | 10.2 | 508 | 0.176 | 168 | 0.870 |

†Characterized by energy-dispersive spectroscopy; ‡BET surface ($S_{BET}$) was Characterized based on the $N_2$ adsorption isotherms obtained at 77 K. Micropore volumes ($V_{mic}$) were estimated based on the V-t method. Mesoporous volumes ($V_{meso}$) were estimated based on the BJH method.

### Materials for synthesis

All materials for synthesizing the *BEA-type zeolites were used as received without further purification from the specified vendors. The moisture contents of the solid-phase reagents were determined through independent temperature gravimetric analyses (TGA). Aluminum sources used in this work included aluminum isopropoxide (Al(*i*-$C_3H_7$)$_3$, ≥98%, Sigma Aldrich) and sodium aluminate (40.0–44.0% $Na_2O$, 46.0–53.0% $Al_2O_3$, DAEJUNG). Silica sources used in this work were fumed silica (Cab-O-Sil®, ACROS) and colloidal silica (LUDOX SM-30, 30% $SiO_2$ dispersed in $H_2O$ Sigma-Aldrich). Mineralizing agents used in this work were ammonium fluoride ($NH_4F$, ≥98%, Sigma-Aldrich), sodium hydroxide solution (65.2 wt.% NaOH in $H_2O$), and sodium hydroxide beads (97%, DAEJUNG). The following organic structure-directing agents (OSDAs) were used as received from the specified vendors: tetraethylammonium hydroxide (TEAOH, 35 wt.% in $H_2O$, SACHEM).

**Zeolite preparation procedures**

All *BEA-type zeolites presented in this work were synthesized using conventional hydrothermal methods, which are modifications of previously reported methods in the literature.[1-3] Initially, Al sources, TEAOH, mineralizers, and distilled water were mixed to achieve a desired gel composition in 40 mL PTFE liners (PlusKoLab). The mixtures were stirred until they became translucent. Subsequently, Si sources were added, ensuring complete dispersion and homogenization through subsequent stirring. The general gel composition can described as 1.0 $SiO_2$ : *x* Al : *y* TEAOH : *z* ($NH_4F$ or NaOH) : *w* $H_2O$. Additional aging steps could be added at this stage, depending on the sample series. The PTFE liners charged with gels were clad in steel autoclaves and transferred to a convection oven preheated to the desired temperature, which could be rotating or static. The progress of crystallization was monitored by analyzing PXRD patterns of aliquots collected every 3–7 days. Following crystallization, the products were thoroughly rinsed with distilled water and acetone consecutively using a centrifuge and then calcined at 580 °C for 6 hours. The resultant *BEA-type zeolites were converted into their H-forms through ion exchange processes with ammonium nitrate (100 ml 1 M $NH_4NO_3$ solution per 1 g zeolite, twice at 80°C for 6 hours) followed by subsequent calcination at 580 °C for 6 hours.

The L (large)-series samples were synthesized using fluoride media.[1] Desired amounts of aluminum isopropoxide, TEAOH solution, and ammonium fluoride were mixed in a PTFE liner, and fumed silica was gradually added and stirred to ensure homogeneous mixing. The final gel composition can be written as 1 $SiO_2$ : *x* Al : 0.45 TEAOH : 0.4 $NH_4F$ : 6.9 $H_2O$, with *x* varying between 0.02 and 0.06. Crystallization was carried out in a rotating oven set at 150 °C for 14 days.

The M (medium)- series samples were synthesized using the following procedure.[2] Desired amounts of sodium aluminate, TEAOH solution, and NaOH solution were mixed in a PTFE liner, and fumed silica was gradually added and stirred to ensure homogeneous mixing. The final gel composition can be written as 1 $SiO_2$ : *x* Al : 0.53 TEAOH : 0.13 NaOH : 21.67 $H_2O$, with *x* varying between 0.01 and 0.08. Crystallization was carried out in a static oven set at 140 °C for 6–11 days.

The S (small)-series samples were synthesized using the following procedure.[3] Desired amounts of aluminum isopropoxide, TEAOH solution, and NaOH beads were mixed in a PTFE liner and colloidal silica was gradually added and stirred to ensure homogeneous mixing. The mixture was stirred for 24 hours at room temperature. The final gel composition can be written as 1 $SiO_2$ : *x* Al : 0.36 TEAOH : 0.014 NaOH : 11.8 $H_2O$, with x varying between 0.006 and 0.05. Crystallization was carried out in a static oven set at 100 °C for 5–22 days.

The detailed gel compositions are presented in Supplementary Table 2.

**Supplementary Table 2. Synthesis conditions of the *BEA-type zeolites shown in this work.**

| Entry | Sample Name | Gel composition | | | | | | Temp. (°C) | Oven Type | Time (days) | Result |
|---|---|---|---|---|---|---|---|---|---|---|---|
| | | $SiO_2$ | Al | TEAOH | NaOH | $NH_4F$ | $H_2O$ | | | | |
| 1 | L-BEA-10 | 1.0 | 0.06 | 0.45 | - | 0.4 | 7.0 | 150 | Rotating | 14 | *BEA |
| 2 | L-BEA-15 | 1.0 | 0.034 | 0.45 | - | 0.4 | 7.0 | 150 | Rotating | 14 | *BEA |
| 3 | L-BEA-20 | 1.0 | 0.03 | 0.45 | - | 0.4 | 7.0 | 150 | Rotating | 14 | *BEA |
| 4 | L-BEA-30 | 1.0 | 0.02 | 0.45 | - | 0.4 | 7.0 | 150 | Rotating | 14 | *BEA |
| 5 | M-BEA-10 | 1.0 | 0.08 | 0.53 | 0.13 | - | 21.7 | 140 | Static | 11 | *BEA |
| 6 | M-BEA-20 | 1.0 | 0.01 | 0.53 | 0.13 | - | 21.7 | 140 | Static | 11 | *BEA |
| 7 | S-BEA-10 | 1.0 | 0.05 | 0.36 | 0.014 | - | 11.8 | 100 | Static | 22 | *BEA |
| 8 | S-BEA-20 | 1.0 | 0.02 | 0.36 | 0.014 | - | 11.8 | 100 | Static | 5 | *BEA |
| 9 | S-BEA-30 | 1.0 | 0.01 | 0.36 | 0.014 | - | 11.8 | 100 | Static | 7 | *BEA |
| 10 | S-BEA-50 | 1.0 | 0.006 | 0.36 | 0.014 | - | 11.8 | 100 | Static | 7 | *BEA |

## Catalytic reaction analysis

**Closed-batch reaction procedure.**
Closed-batch catalytic cracking was carried out using a stirring batch reactor (ChemReSys, R-201). Initially, 1 g of zeolite catalyst and 10 g of model feed polyethylene (LDPE, melt index 25 g/10 min at 190 °C/2.16 kg, Sigma-Aldrich, Mw~204,000 by GPC) were placed in a 75 mL stainless steel liner and sealed within the stirring reactor. The reaction proceeded for 2 hours at a bulk temperature of 330 °C with stirring at 200 rpm. After 2 hours, the outlet valve was released, and the liquid product was collected via a condensation device connected to a cold constant-temperature circulation column set at -15 °C, utilizing two stages to minimize process loss. The gaseous product was collected in a gas sampling bag connected to the end of the reactive distillation setup and analyzed using a GC-FID.

**Quantification of gas products procedure.**
Quantification of gas products involved measuring the volume of the gas sampling bag and quantifying the $C_{1\text{-}7}$ products using a GC-FID. The volume of the gas sampling bag was determined by the water displacement method. A beaker was filled with water and the gas sampling bag was submerged. The volume of gas products was defined as the difference between beaker and the volume displaced by the gas sampling bag. The concentrations of each gas species were determined using a GC-FID with calibrations curves of the individual gas products.

**Data analysis and quantification**
Conversion of LDPE and quantification of the liquid products ($C_{5\text{–}30}$) was calculated from the GC-FID with a calibration curve of C7–C30 saturated alkanes (1000 μg/ml each component in hexane, Sigma Aldrich). The liquid product resulting from the catalytic cracking of LDPE comprised numerous isomers and aromatic compounds. Identifying every peak is challenging, so the signals were categorized into groups based on carbon numbers. The mean retention time of each standard n-alkane served as the reference line for dividing the carbon number groups. Subsequently, the calculation of liquid product hydrocarbons involved integrating the area by groups and utilizing the calibration curve. Conversion of LDPE was calculated using the following equation and quantification of the products was determined from the GC-FID

$$\text{The weight of residue} = \text{the weight of liner after reaction} - \text{the weight of empty liner} - \text{the weight of catalyst}$$

$$\text{The weight of liquid products} = \text{the weight of liquid reservior after reaction} - \text{the weight of empty reservoir}$$

$$\text{Conversion (\%)} = \frac{the\ weight\ of\ virgin\ reactant\ -\ the\ weight\ of\ residue}{the\ weight\ of\ virgin\ reactant} \times 100$$

$$\text{Liquid selectivity (\%)} = \frac{\text{the weight of liquid products}}{the\ weight\ of\ virgin\ reactant - the\ weight\ of\ residue} \times 100$$

$$\text{Yield (\%)} = \frac{the\ weight\ of\ C_i}{the\ weight\ of\ liquid\ products\ (C_{5-30})} \times 100$$

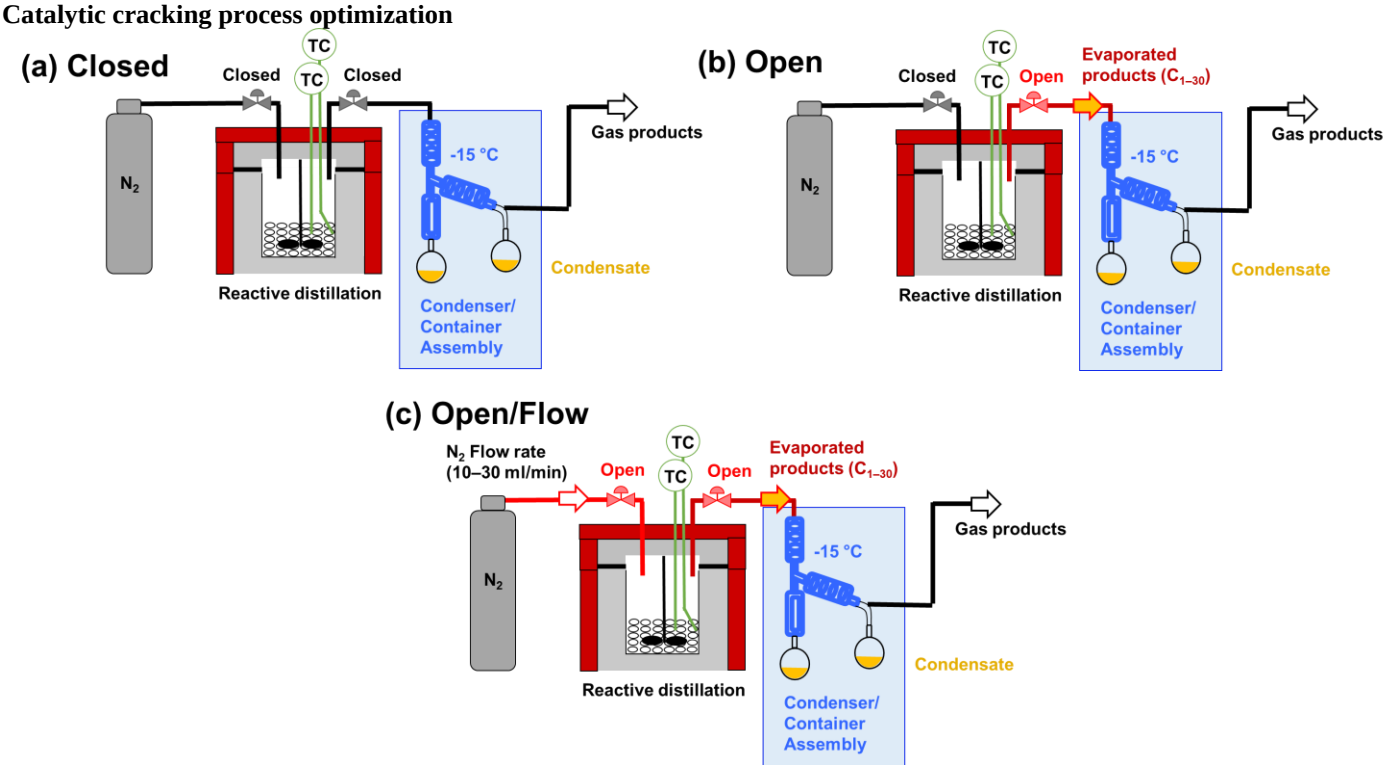


**Supplementary Figure 3. Three operation modes of the open-batch reactor system used in this work:** (a) closed-batch mode, (b) open-batch/no-flow mode, and (c) open-batch/flow mode.

The semi-batch reactor used in this work was designed to operate in either closed-batch or open-batch mode. The selection can be made by simply switching the 2-way ball valve that regulates the product flow between the reactor and the condenser/container assembly. The effects of batch operation modes were tested using selected zeolite beta ("S-BEA-30" sample (see below), EDS Si/Al ~ 28, particle size ~110 nm) with a PE/zeolite ratio of 10 at 330 °C for 2 hours without inert gas flow.

Supplementary Figure 3 shows the operation modes of the semi-batch reactor used in this work. In the closed batch (Supplementary Figure 3(a)), PE feed and hydrocarbon products are in contact with the zeolite throughout the entire reaction time. In this mode, the conversion and liquid selectivity were 38.3% and 44.9%, respectively (Figure 2(a), main text). These values increased to 45.1% and 65.3% when the reactor operated in the open-batch/no-flow mode (Supplementary Figure 3(b)), respectively. In this open-batch/no-flow operation mode, the volatile components that can evaporate at the reaction temperature (here, 330 °C) can escape the reactor with a shorter contact time, preventing overreaction over zeolite surfaces that forms gas species and solid coke species.

When an inert gas ($N_2$) flow was introduced from the reactor inlet (Supplementary Figure 3(c)), under the same reaction conditions, the conversion and liquid selectivity improved further; with an $N_2$ gas flow rate of 10 mL·min$^{-1}$, the conversion and liquid selectivity increased to 52.2% and 64.2%, respectively. However, the conversion further increased to 58.5% when the $N_2$ gas flow rate was 30 mL·min$^{-1}$, but the liquid selectivity decreased to 54.0%. This decrease is presumably due to the loss of evaporated liquid fraction escaping the condenser/container assembly because of the high flow rate of inert carrier gas. The product distribution in the condensate (Figure 2(b), main text) clearly shows that the decrease in contact time (the increase in inert gas flow rate) effectively increases the mean molecular weight of the liquid products, indicating reduced overreaction that forms gas-phase products.
These results imply that liquid product selectivity can be improved and modified based on the proper batch reactor setup, even with the same catalyst and reaction temperature/time.

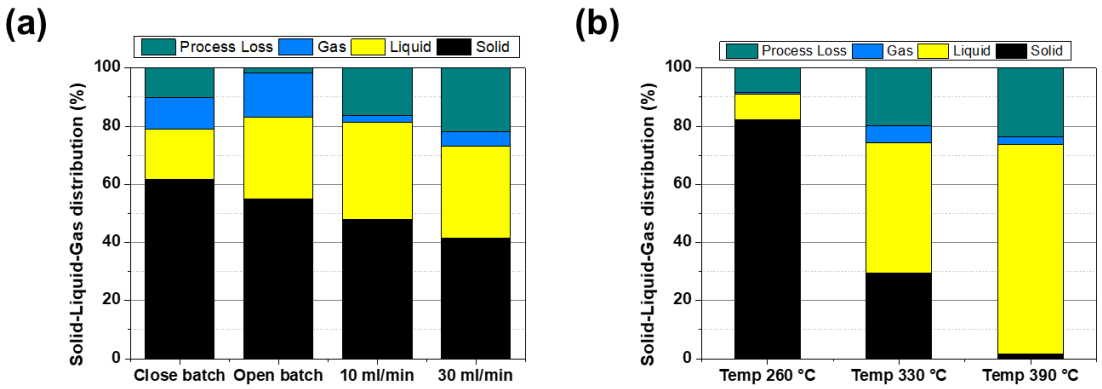


**Supplementary Figure 4. Solid-liquid-gas distribution from the open-batch PE catalytic cracking:** (a) using S-BEA-30 with varied reactor configuration, (b) using S-BEA-20 with varied reaction temperature configuration. Small crystal sized zeolite beta with y (Si/Al) denoted as S-BEA-y

Some degree of "process loss" (0–20 %) was inevitable in all catalytic runs, attributed to the small-scale and non-steady-state nature of the reaction process. The process loss primarily consisted of gaseous species and minor amounts of liquid volatiles. The solid phase was quantified using a balance. Thus, the reliability of quantified data is ranked as follows: solid > liquid > gas.

**Supplementary data for the commercial zeolite experiments**

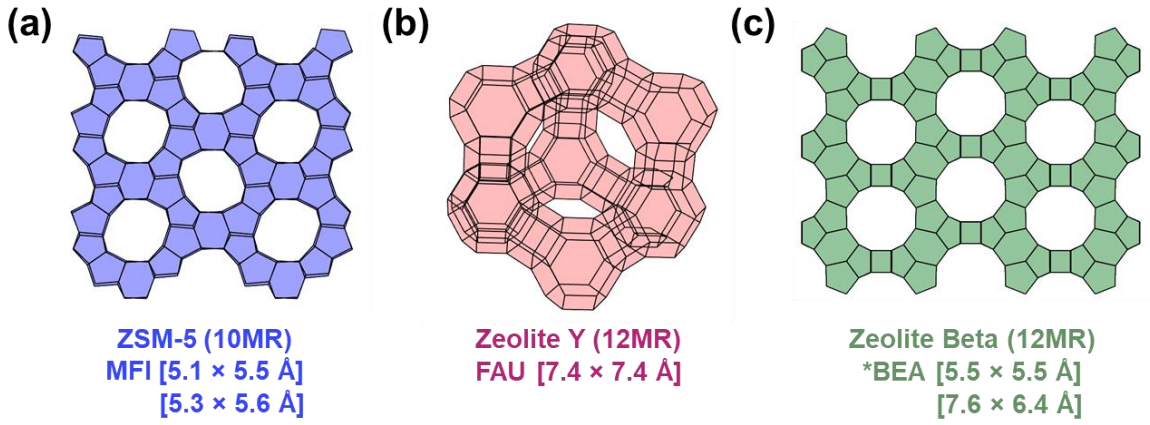


**Supplementary Figure 5. Structures of commercial zeolites demonstrated in this work:** (a) ZSM-5, (b) Zeolite Y, (c) Zeolite Beta

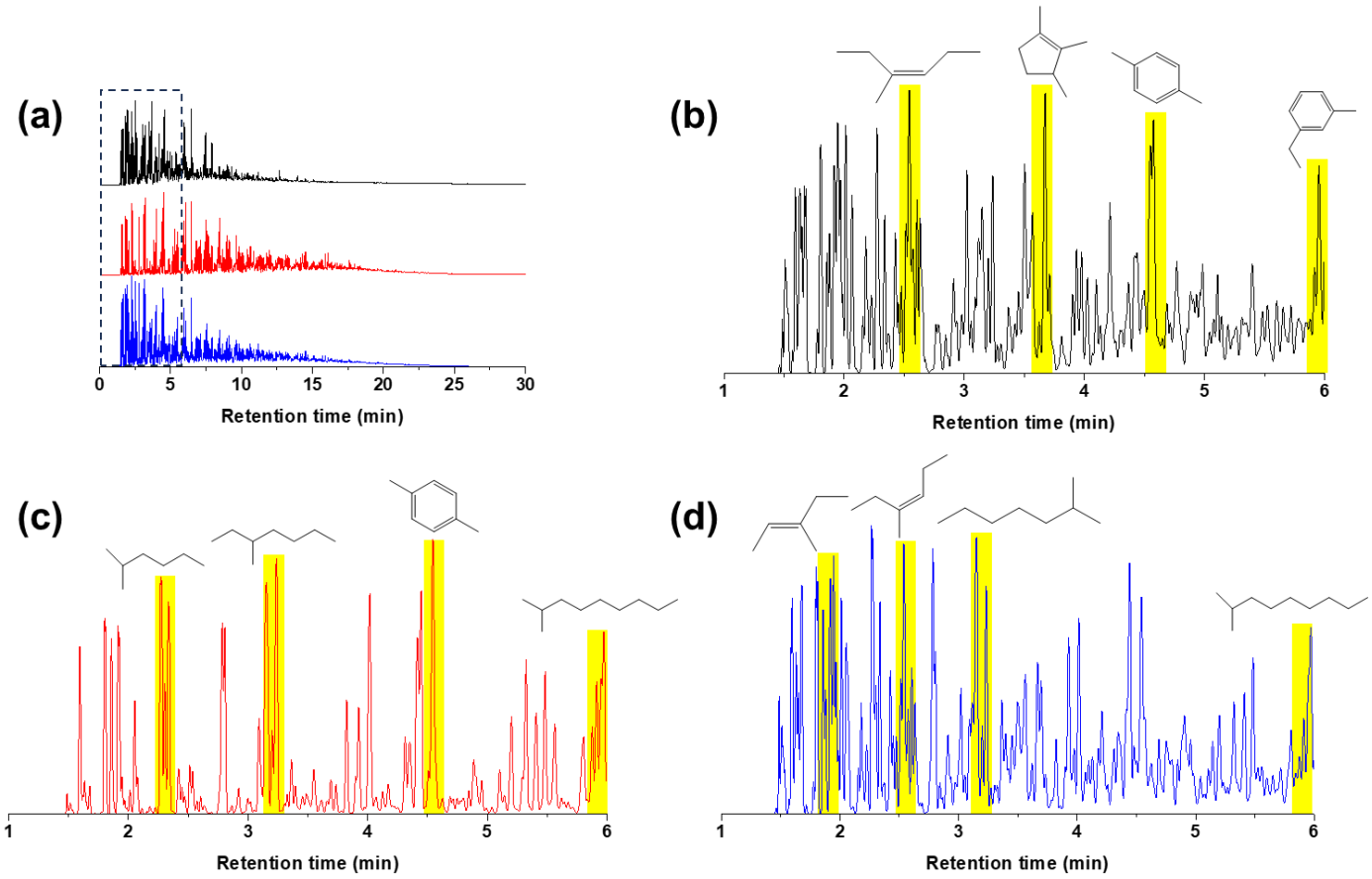


**Supplementary Figure 6. Gas chromatography (GC) profiles of the liquid products from 330°C open-batch polyethylene catalytic cracking with commercial zeolites:** (a) complete chromatograms (Black: ZSM-5, Red: zeolite Y(1), Blue: zeolite beta); (b-d) magnified GC regions (1–6 min) with the major products identified using mass spectrometry (MS) for ZSM-5, zeolite Y(1), and zeolite beta, respectively. Hydrocarbons with the highest quantitative composition in the GC region of the major products are highlighted in yellow.

The complexity of chromatograms suggests extensive isomerization by Brønsted acid sites of zeolites. Zeolites with larger pore openings (12MR, zeolite Y and zeolite beta) produced liquid products with heavier components than those produced over ZSM-5 (10MR), as evidenced by the complete chromatograms shown in Supplementary Figure 6(a). This indicates the influence of micropores in PE catalytic cracking. Particularly, the identification of light hydrocarbons obtained at early retention times using GC-MS revealed distinctly different chemical species distributions. This demonstrates the influence of the shape selectivity of the micropores of the zeolites used.

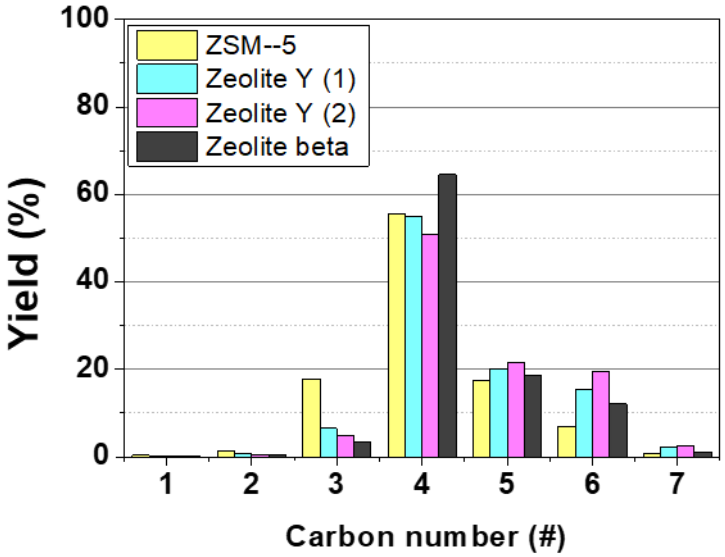


**Supplementary Figure 7. Gas product selectivity distributions from various commercial zeolites.**

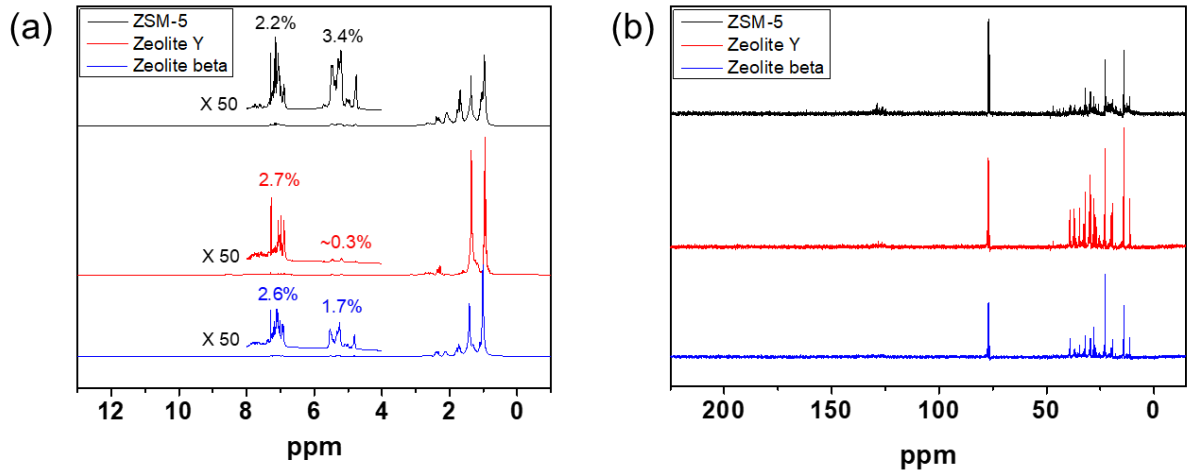


**Supplementary Figure 8. Nuclear magnetic Resonance (NMR) spectra of liquid products from the open-batch polyethylene catalytic cracking using various structure zeolites: (a) $^{1}$H NMR and (b) $^{13}$C NMR.**

To further analyze the nature of the liquid product mixture obtained from open-batch PE cracking at 330 °C over ZSM-5, zeolite Y, and zeolite beta, $^{1}$H and $^{13}$C solution NMR analyses were conducted. The NMR analyses were performed using a 300 MHz Bruker AVANCE III HD (Bruker, Germany) magnet with a 5 mm probe. The content of olefinic (vinyl) $sp^2$ C-H protons showed significant differences among the three frameworks. Olefinic protons were most abundant in the order of ZSM-5 > zeolite beta > zeolite Y, consistent with the conversion trends in open-batch PE cracking. On the other hand, aromatic $sp^2$ C-H protons exhibited a relatively weaker trend, with a content of approximately 2.2–2.7%.

**Supplementary data for the various *BEA-type zeolite experiments**

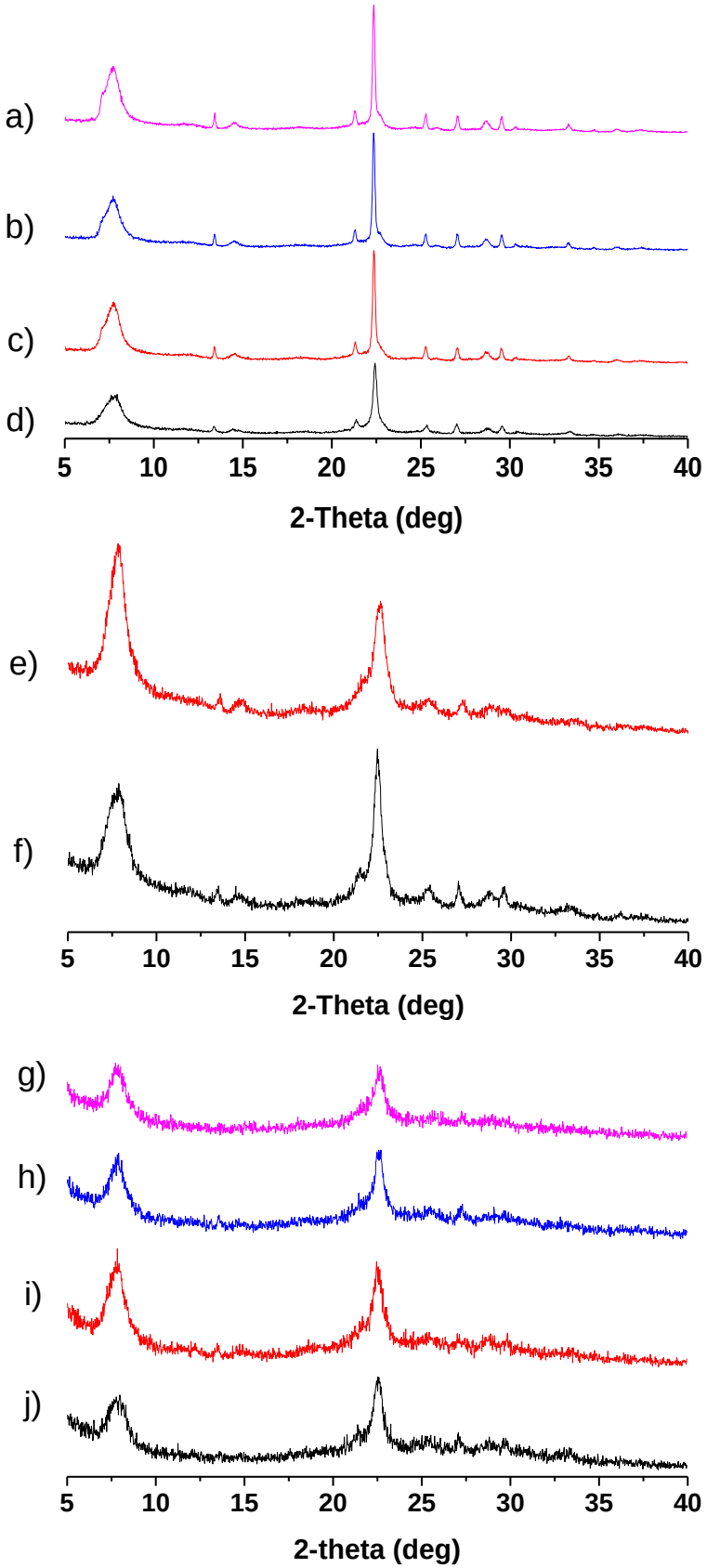


**Supplementary Figure 9. Powder X-ray diffraction profiles of synthesized beta zeolites:** (a) L-BEA-30, (b) L-BEA-20, (c) L-BEA-15, (d) L-BEA-10, (e) M-BEA-20, (f) M-BEA-10, (g) S-BEA-50, (h) S-BEA-30, (i) S-BEA-20, and (j) S-BEA-10. Large, Medium, Small crystal sized zeolite beta with y (Si/Al) denoted as L-, M-, S-BEA-y

The L-series samples exhibited relatively sharp and well-defined diffraction peaks, whereas the M-series and S-series displayed broader diffraction signals, suggesting smaller *BEA crystalline domain sizes.

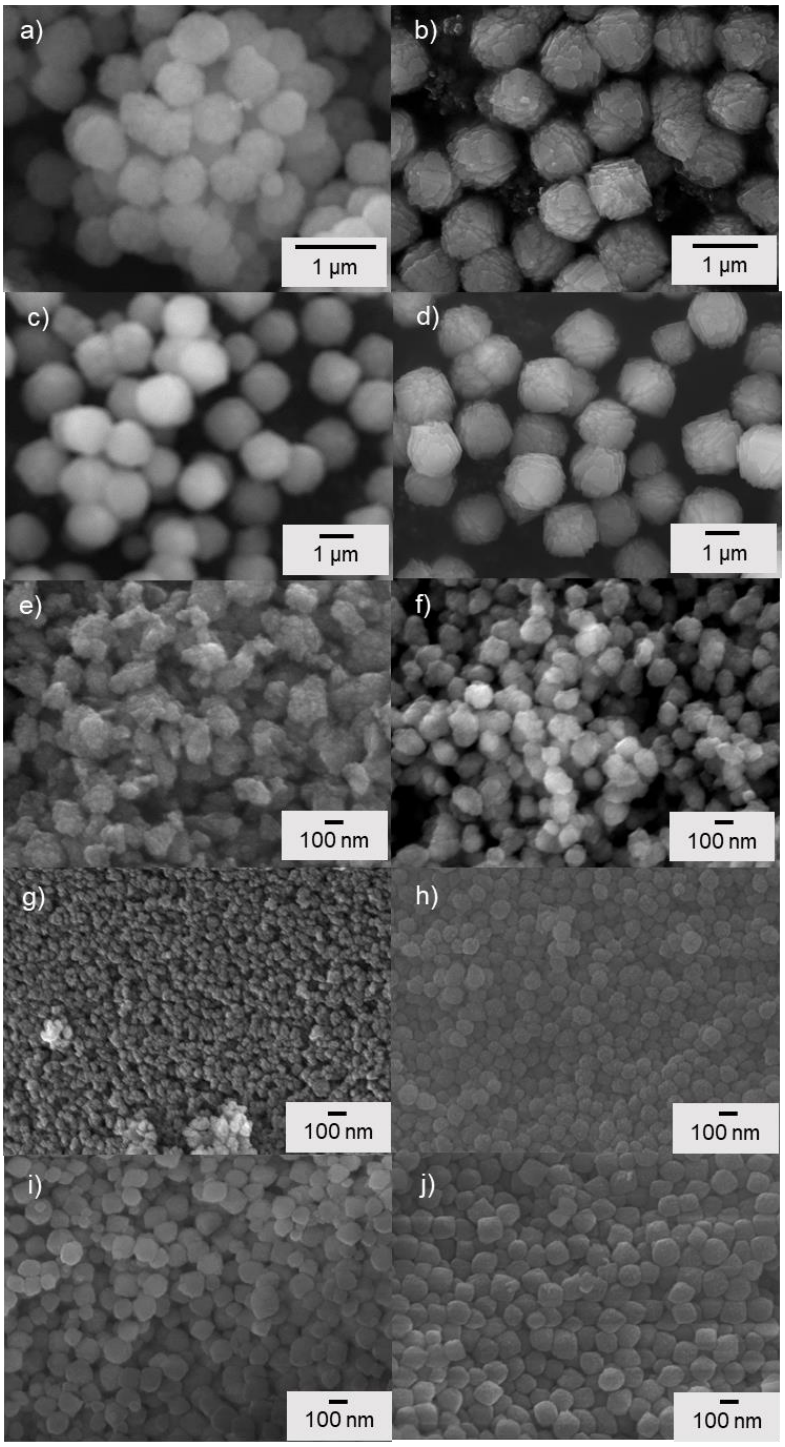


**Supplementary Figure 10. Scanning electron microscope images of intrinsic properties-controlled beta zeolites:** (a) L-BEA-10, (b) L-BEA-15, (c) L-BEA-20, (d) L-BEA-30, (e) M-BEA-10, (f) M-BEA-20, (g) S-BEA-10, (h) S-BEA-20, (i) S-BEA-30, and (j) S-BEA-50. Large, Medium, Small crystal sized zeolite beta with y (Si/Al) denoted as L-, M-, S-BEA-y

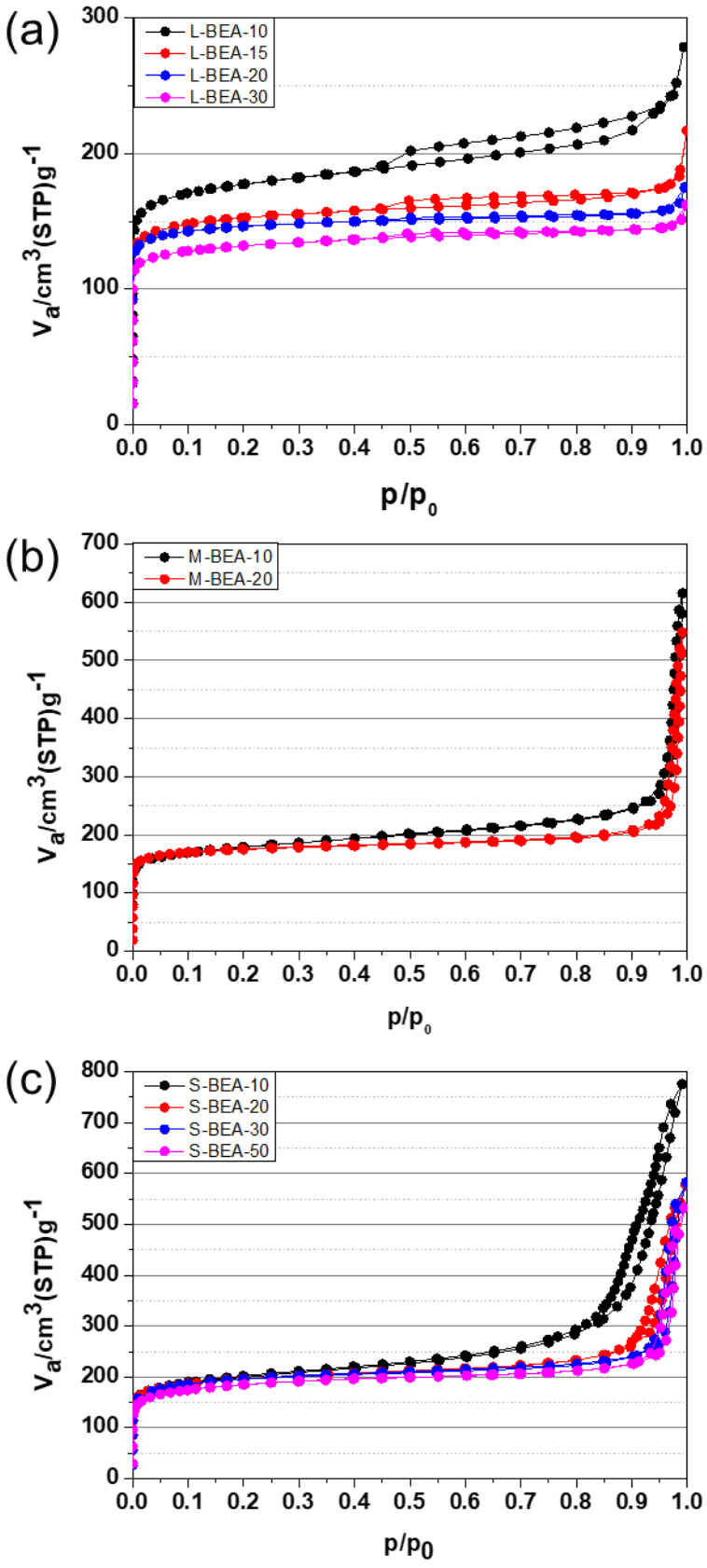


**Supplementary Figure 11. 77 K $N_2$ adsorption and desorption isotherms of the prepared *BEA-type zeolite series:** (a) L-series, (b) M-series, and (c) S-series. Large, Medium, Small crystal sized zeolite beta with y (Si/Al) denoted as L-, M-, S-BEA-y

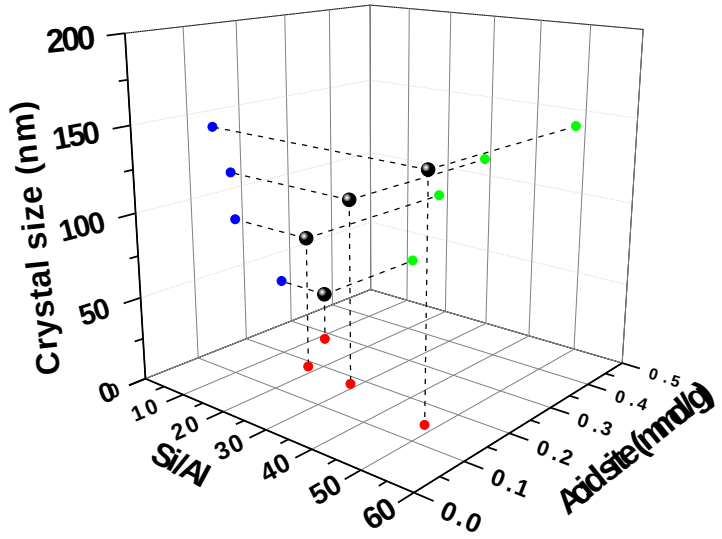


**Supplementary Figure 12. Correlation between Si/Al ratio, Brønsted acid site and crystal size of small crystal sized zeolite beta.** The direct linear correlation was calculated with quantified Bronsted acid sites, Si/Al and crystal size within zeolites using $NH_3$-temperature-programmed desorption analysis, scanning electron microscopy with energy-dispersive spectroscopy.

To investigate the correlation between Brønsted acid sites, Si/Al ratio, and crystal size in the context of open-batch catalytic cracking, we conducted $NH_3$-TPD (Ammonia Temperature-Programmed Desorption) analysis.[4] The $NH_3$-TPD measurements were performed using an AutoChem II (Micromeritics Inc.) instrument. For each zeolite sample, 30 mg was pretreated at 400°C for 1 hour under a helium (He) stream to remove any adsorbed impurities. After pretreatment, $NH_3$ (5% balanced with He) was introduced at 100°C to saturate the sample. Following saturation, the flow was switched back to He to eliminate any physiosorbed $NH_3$. The TPD analysis was then carried out by heating the sample to 600°C at a rate of 10°C/min, and the desorbed $NH_3$ was monitored using a thermal conductivity detector (TCD).

As shown in Supplementary Figure 12, we analyzed Brønsted acid sites in S-Series zeolite beta and examined their relationship with Si/Al ratio and crystal size. The results indicate that the quantity of Brønsted acid sites follows a similar trend to the Si/Al ratio. This suggests that the Al content introduced during synthesis is not merely present in the framework but is effectively incorporated as Brønsted acid sites, which act as strong acid sites during catalytic cracking.

Furthermore, we observed that as the Si/Al ratio decreases and the number of Brønsted acid sites increases, there is a corresponding reduction in crystal size. This indicates that smaller crystal sizes are associated with higher concentrations of Brønsted acid sites, likely due to the increased availability of external acid sites in smaller crystals. These findings highlight a clear correlation between Si/Al ratio, Brønsted acid site, and crystal size, providing valuable insights into how these factors influence catalytic performance in open-batch setups.

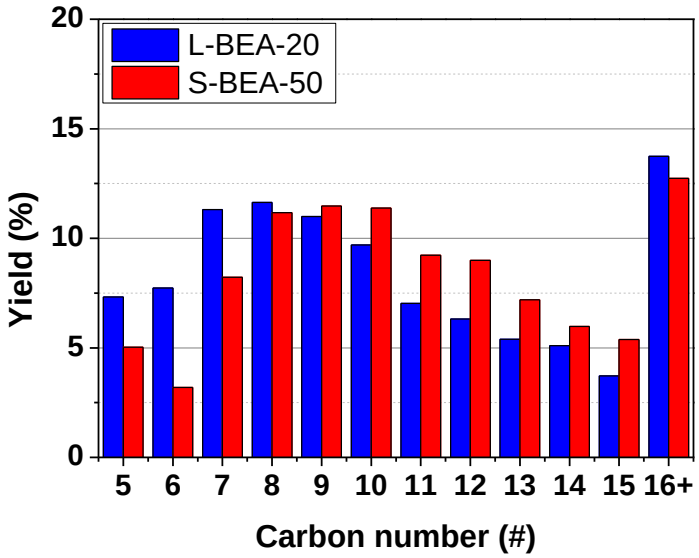


**Supplementary Figure 13. Hydrocarbon distribution in liquid products from intrinsic properties-controlled beta zeolite catalytic cracking of low-density polyethylene at 330 °C, 2 h, 10 ml $N_2$/min.** Large, Small crystal sized zeolite beta with y (Si/Al) denoted as L-, S-BEA-y

In catalytic cracking, the distribution of decomposition products is influenced by conversion, with higher conversion leading to more C-C bond cleavage and, consequently, lighter products. Therefore, comparing product distributions at similar conversion levels allows for a clearer understanding of the effect of crystal size on product distribution. S-BEA-50 and L-BEA-20, despite differing in crystal size and Si/Al ratio, both exhibited approximately 40% conversion. At similar degrees of decomposition, Supplementary Figure 13 illustrates the shift in product distribution due to crystal size differences. Specifically, S-BEA-50, with its smaller crystal size, shows a shift toward longer-chain hydrocarbon products. This suggests that, despite higher Si/Al ratio, the larger external surface area of S-BEA-50 compensates for the fewer acid sites. Consequently, it can be concluded that smaller crystal sizes, which provide more external acid sites, significantly influence product distribution.

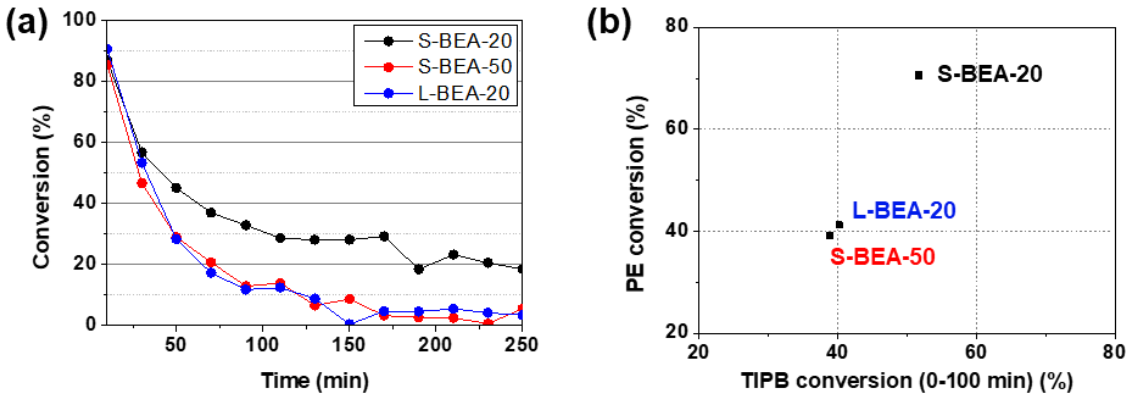


**Supplementary Figure 14. 1,3,4-Triisopropylbenzene (TIPB) cracking results over selected zeolite beta samples with different intrinsic properties**: (a) TIPB cracking time-on-stream plots of S-BEA-20, S-BEA-50, L-BEA-20 and (b) initial TIPB conversion compared against polyethylene (PE) conversion. Large, Medium, Small crystal sized zeolite beta with y (Si/Al) denoted as L-, M-, S-BEA-y.

To justify comparing the cracking behavior of zeolite beta sample series synthesized through different methods, we conducted independent 1,3,5-triisopropylbenzene (TIPB) cracking experiments on three selected samples. TIPB, with a kinetic diameter of 9.5 Å, cannot enter the 7.5 Å pore openings of zeolite beta.[5] Therefore, we hypothesized that TIPB conversion during cracking would relate to the external acid site density of zeolite beta. We applied TIPB cracking to the S-BEA-20 (reference), S-BEA-50, and L-BEA-20 samples and compared the results with the cracking behavior of model PE. S-BEA-50 has fewer acid sites than S-BEA-20, while L-BEA-20 has a much larger particle size than S-BEA-20. S-BEA-50 and L-BEA-20 possess completely different Si/Al ratios and crystal sizes and are synthesized through different methods. However, at 330 °C, the PE conversion rates from S-BEA-50 and L-BEA-20 were very similar, at 39.1% and 41.2%, respectively. Therefore, we believed that if S-BEA-50 and L-BEA-20 exhibited similar behavior in TIPB cracking, it would justify comparing zeolite beta samples produced by different synthesis methods.

TIPB cracking was conducted under the following conditions: reaction temperature = 400 °C, feed rate = 8 µl TIPB/min, carrier gas = 100 mL $N_2$/min, bed composition: zeolite beta samples (100 mg) mixed with quartz sand (300 mg), and pretreatment: 400 °C for

1 hour. S-BEA-20 showed a higher TIPB conversion (51.7%) compared to the other two samples. S-BEA-50 and L-BEA-20 achieved similar TIPB conversion levels (Supplementary Figure 14(a)), with initial TIPB conversions of 38.9% and 40.2%, respectively. Since TIPB cracking, which results in the loss of propylene, occurs only at external Brønsted acid sites, we can infer that S-BEA-50 and L-BEA-20, synthesized by completely different methods, have similar external surface acid site densities. Additionally, the PE conversion presented in Figure 4(a) of the main text also shows similar results for S-BEA-50 and L-BEA-20. (Supplementary Figure 14(b)) Therefore, it can be proposed that despite different synthesis methods, PE conversion influenced by external acid site density can be equivalently evaluated.

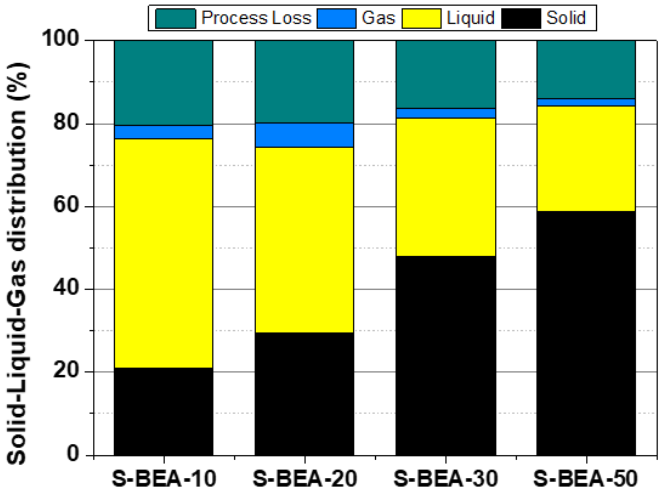


**Supplementary Figure 15. Solid-liquid-gas distribution from the 330°C open-batch polyethylene catalytic cracking with the S-series catalyst with varied Si/Al ratio.** Small crystal sized zeolite beta with y (Si/Al) denoted as S-BEA-y.

The "process loss" mainly consisted of gaseous species and small amounts of liquid volatiles, which was inevitable due to the small-scale, non-steady-state nature of the open batch reactor system, as mentioned above. An increase in the Si/Al ratio led to a larger amount of remaining solid phase, as shown in Supplementary Figure 15. suggesting that less acid sites in the system resulted in a sluggish PE decomposition.

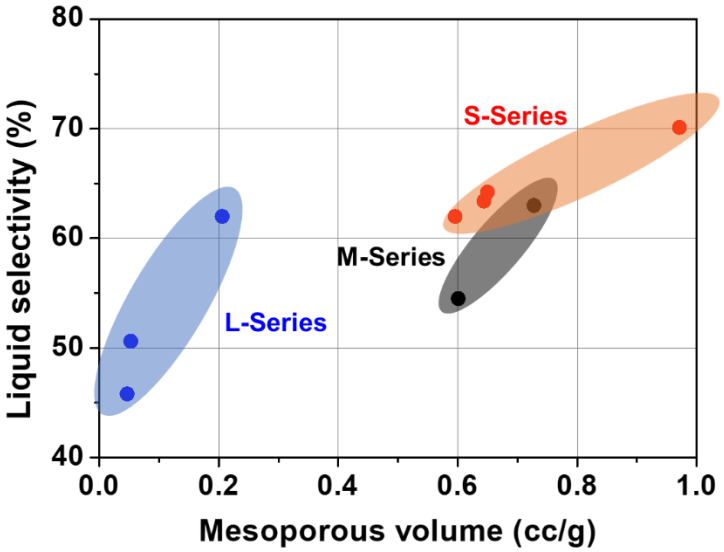


**Supplementary Figure 16. Relationship between mesoporous volume and liquid selectivity for intrinsic properties-controlled beta zeolite including L-Series, M-Series, S-Series.** Large, Medium, Small crystal sized zeolite beta denoted as L-, M-, S-series, respectively.

As shown in Table 1, an increase in external surface area is accompanied by a corresponding rise in mesoporous volume of zeolites. In the catalytic cracking conducted in this study, the external surface acid sites of the catalyst play a crucial role, and the presence of mesopores also significantly influences the reaction outcomes. Supplementary Figure 16 demonstrates a clear trend: an increase in mesoporous volume leads to higher liquid product selectivity.

The increase in mesoporosity within zeolites reduces diffusion limitations for long-chain hydrocarbons, which are formed by ß-scission of polyethylene at external acid sites, thereby facilitating access to micropore Brønsted acid sites.[6] This enhancement also enables efficient recovery of cracking products through inert carrier gas flow, thus enhancing catalytic activity and liquid product selectivity while minimizing coke formation.

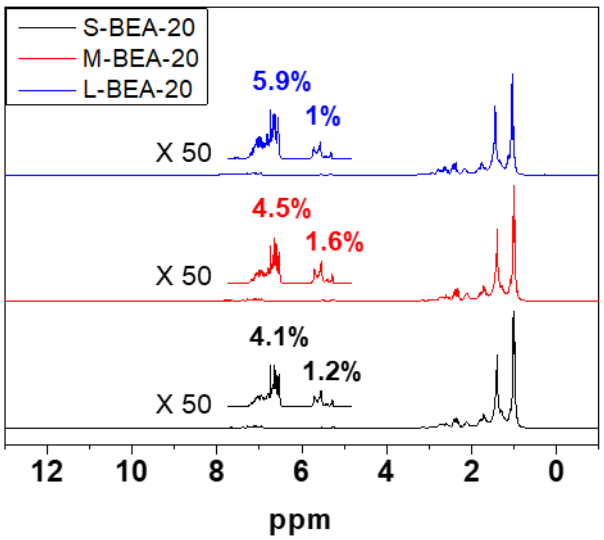


**Supplementary Figure 17. $^{1}$H Nuclear Magnetic Resonance (NMR) spectra of liquid products from catalytic cracking with open-batch setup using intrinsic properties-controlled zeolite beta.** Large, Medium, Small crystal sized zeolite beta with y (Si/Al) denoted as L-, M-, S-BEA-y.

To further investigate the distribution of aromatic, olefinic, and aliphatic compounds in the liquid products obtained from catalytic cracking of PE using S-Series, M-Series, and L-Series zeolite beta, we performed additional $^{1}$H-NMR analysis. As shown in Supplementary Figure 17, the aromatic $sp^2$ C-H signals (6-8 ppm) were found to be more prominent in larger crystal-sized zeolites: L-Series (5.9%) > M-Series (4.5%) > S-Series (4.1%). This trend suggests that larger crystals promote the formation of aromatic compounds during PE cracking. The increased formation of aromatics may be attributed to the increased relative contribution of micropore acid sites, where micropores provide shape selectivity favorable for aromatization. Larger crystals are also capable of providing prolonged residence time that leads to a higher chance to aromatization.

Conversely, in smaller crystal-sized zeolites (S-Series), a higher proportion of external acid sites facilitates more efficient ß-scission of polymer chains at these external sites. Due to the open-batch reactor setup, the cracked products are quickly desorbed and recovered by the carrier gas before undergoing coke formation inside the micropores, resulting in lower aromatic content. The olefinic proton signals were relatively weak across all samples, ranging from 1-1.6%, indicating minimal variation in aromatics/olefin production between different zeolite sizes.

This analysis supports our hypothesis that smaller crystal-sized zeolites with enhanced external acidity promote selective cracking of polymers while suppressing undesired aromatization, leading to a higher yield of non-aromatic liquid products.

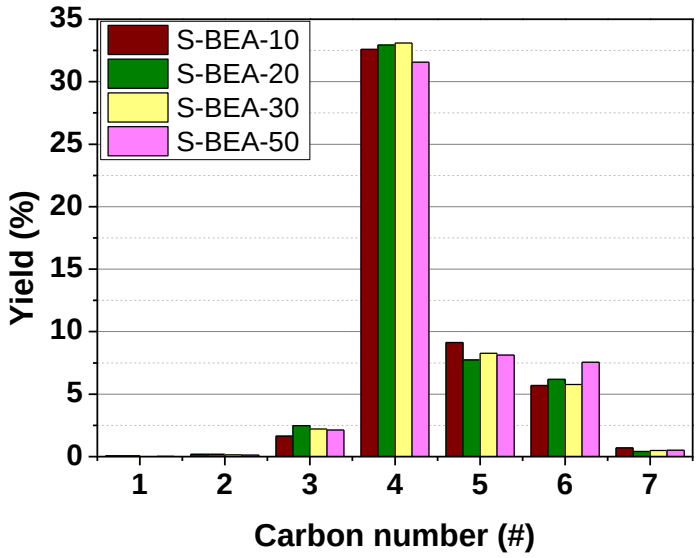


**Supplementary Figure 18. Gas product selectivity distributions from the S-BEA series catalysts.** Small crystal sized zeolite beta with y (Si/Al) denoted as S-BEA-y.

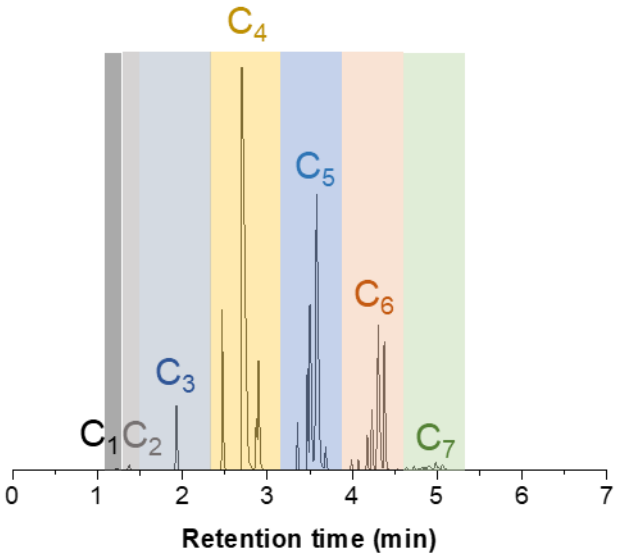


**Supplementary Figure 19. Gas chromatography chromatogram of gas products from the open-batch polyethylene catalytic cracking using S-BEA-20.** Small crystal sized zeolite beta with y (Si/Al) denoted as S-BEA-y.

Hydrocarbon gas products from the $C_4$ group were produced in the highest quantities, and the volatile light hydrocarbons in the $C_{5\text{-}7}$ range were also identified among the gaseous products.

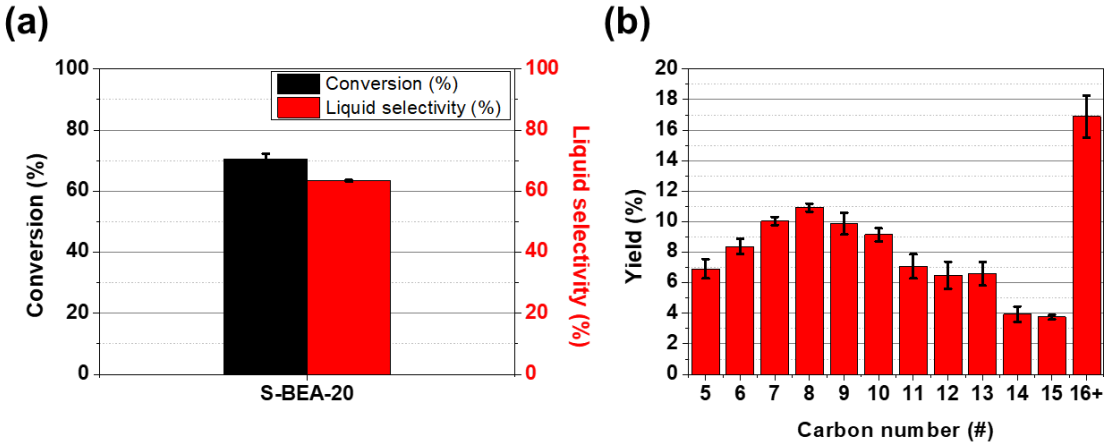


**Supplementary Figure 20. The results of catalytic cracking using S-BEA-20 with error bars:** (a) polyethylene conversion, liquid selectivity, and (b) liquid product selectivity distributions with S-BEA-20 catalyst. Error bar was calculated via standard deviation of three parallel tests. Small crystal sized zeolite beta with y (Si/Al) denoted as S-BEA-y.

To ensure the reliability and reproducibility of our findings, replicate experiments were conducted using S-BEA-20 catalysts. The results from these catalytic cracking experiments demonstrated a high degree of consistency, with variations within a 5% error margin for each individual result. This confirms the feasibility and robustness of our experimental approach and supports the validity of the observed catalytic performance.

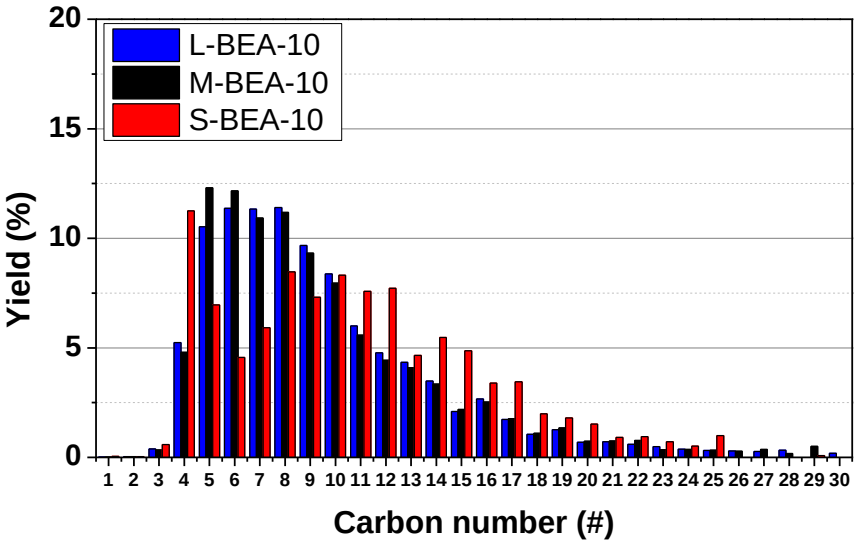


**Supplementary Figure 21. Hydrocarbon full distributions in liquid & gas products from open-batch catalytic cracking with L-Series, M-Series, S-Series.** Large, Medium, Small crystal sized zeolite beta with y (Si/Al) denoted as L-, M-, S-BEA-y.

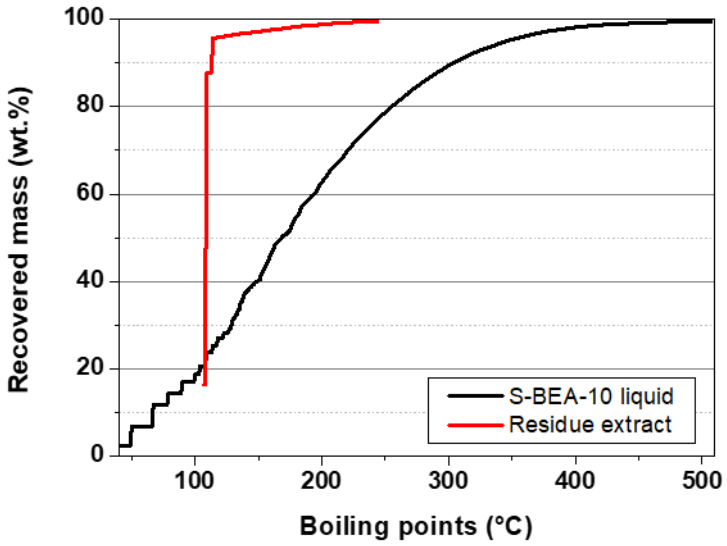


**Supplementary Figure 22. Simulated distillation profiles of the liquid product obtained from the 330 °C catalytic cracking using S-BEA-10 catalyst and the residue toluene extract.** Small crystal sized zeolite beta with y (Si/Al) denoted as S-BEA-y.

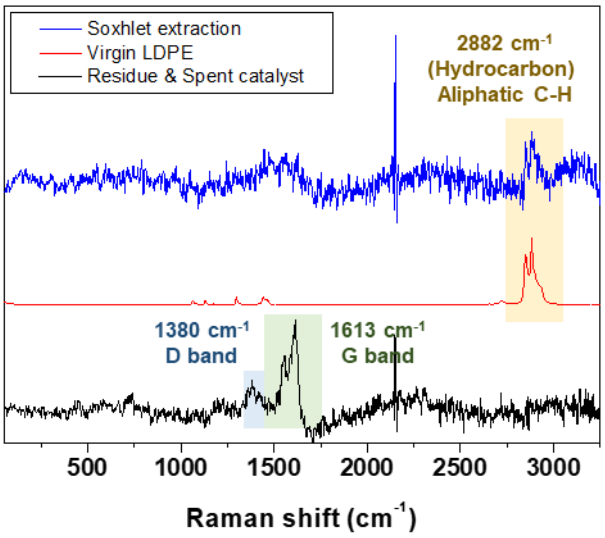


**Supplementary Figure 23. Raman spectra of the residue toluene extract, the virgin low-density polyethylene, and the post-reaction solid phase recovered from the reaction.**

**Supplementary Table 3. Selectivity distribution in liquid products.**

| Sample | $C_5$–$C_{10}$ (naphtha) | $C_{10}$–$C_{20}$ (middle distillate) | $C_{20}$–$C_{30}$ (light vacuum gas oil) | $C_{30}$–$C_{40}$ (heavy vacuum gas oil) | $C_{40+}$ (residue) |
|---|---|---|---|---|---|
| S-BEA-10† | 45.4 | 49.8 | 4.9 | 0 | 0 |
| S-BEA-10‡ | 53.2 | 41.5 | 4.4 | 0.9 | 0 |
| Residue extraction‡ | 98.1(toluene) | 1.9 | 0 | 0 | 0 |

†Characterized by gas chromatography-flame ionization detector; ‡Characterized based on Simulated distillation (SIMDIS).

To analyze the remaining solid phase composed of spent catalysts and solid hydrocarbons formed after catalytic cracking, Soxhlet extraction was conducted with toluene as the solvent at 110 °C under reflux. The Soxhlet extraction process was maintained for a duration of 8 hours. The boiling toluene vapor condensed upon contact with the water-cooled condenser, dripping back into the extraction chamber to dissolve the soluble components. This cycle was repeated continuously, facilitating thorough extraction. Analysis of the extract solution by simulated distillation (SIMDIS) revealed it was composed almost entirely of solvent (Supplementary Table 3), indicating the residue contained uncracked LDPE or coke. The Raman spectrum of the post-reaction solid phase (Supplementary Figure 23) indicates that the solid mixture mostly exhibits characteristics of graphitic coke, which may have deposited on the zeolite surface. This is supported by the negligible intensity of the absorption band for aliphatic C-H vibration, suggesting that aliphatic compounds barely survive during the reaction.

Also, the quantification of the liquid product obtained from the cracking experiments using the S-BEA-10 catalyst was cross-verified using GC-FID and SIMDIS. It was confirmed that the majority of the acquired liquid product is indeed within the $C_5$ to $C_{30}$ range.

**Supplementary data for the catalyst regeneration**

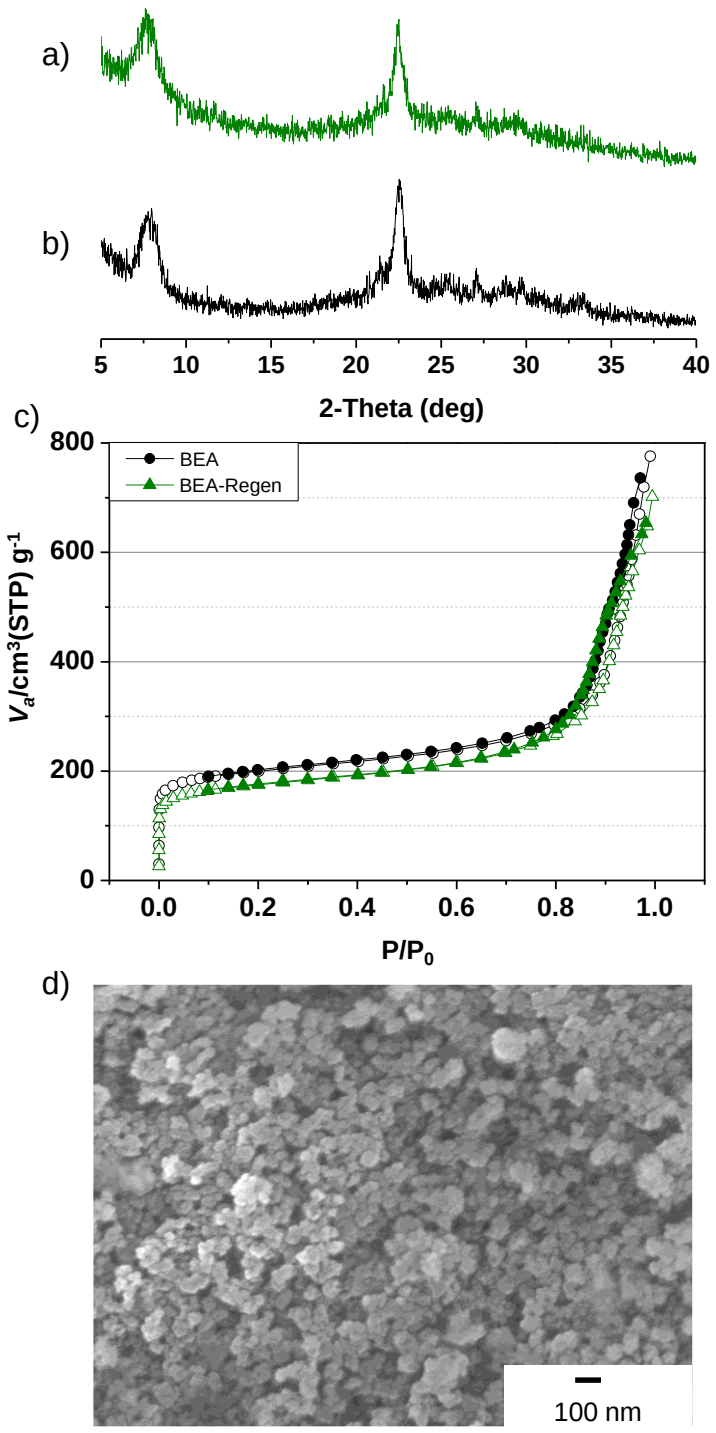


**Supplementary Figure 24. Characterization of regenerated beta zeolite:** (a) Powder-X ray diffraction (XRD) profile of regenerated S-BEA-10, (b) powder-XRD profile of pristine S-BEA-10, (c) $N_2$ adsorption isotherms of pristine and regenerated S-BEA-10, (d) scanning electron microscope image of regenerated S-BEA-10. Small crystal sized zeolite beta with y (Si/Al) denoted as S-BEA-y.

**Supplementary data for the effect of PE feeds**

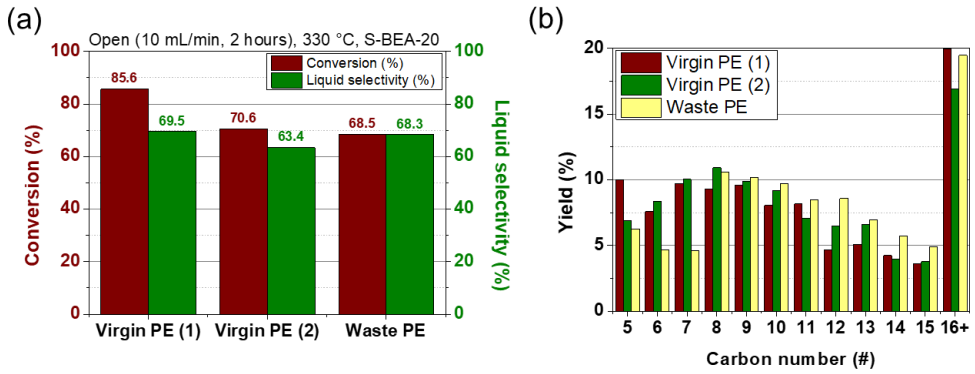


**Supplementary Figure 25. The open-batch (10 mL/min, 2 hour) catalytic cracking behaviors by polyethylene (PE) feed sources:** (a) the conversion and liquid selectivity data and (b) liquid product selectivity distribution from Virgin PE(1) (Mw: 4 kDa), Virgin PE(2) (Mw: 204 kDa by gel permeation chromatography), and actual waste PE. Small crystal sized zeolite beta with y (Si/Al) denoted as S-BEA-y.

To investigate the effects of the molecular weight of the model feed PE on catalytic cracking behavior in this open-batch catalysis setup, we used a low molecular weight PE (4 kDa, denoted as Virgin PE(1) above), which is significantly smaller than the model PE used in this work (204 kDa by GPC, denoted as Virgin PE(2) above). This low molecular weight PE is commonly adopted in many previous studies on the valorization of PE waste.[7,8] As shown in the figure above, the low molecular weight PE exhibited higher conversion and liquid selectivity (85.6% and 69.5%, respectively) than the high molecular weight model PE (70.6% and 63.4%, respectively) under the same standardized open batch catalysis conditions (10 mL/min flow, 2 hours, 330 °C, using the S-BEA-20 zeolite catalyst). Additionally, the liquid product selectivity distribution showed a small dependency on the initial molecular weight of the model PE. These results indicate that the initial molecular weight does influence the catalytic cracking outcomes.

Also, an actual post-consumer PE waste sample (impurities: Ca 2477.890 ppm, Ti 932.288 ppm, Si 463.216 ppm, Pb 254.981 ppm), collected from a regional waste recycling center in Anseong, Gyeonggi-do, South Korea, was also subjected to a catalytic test using the S-BEA-20 catalyst and compared to the case of the model feed of this work (Virgin PE(2)). It achieved a conversion of 69% and a liquid selectivity of 69% under the same conditions. Notably, the product distribution differed, likely due to variations in the molecular weight of the PE as indicated above.

**Comparison to other previous works**

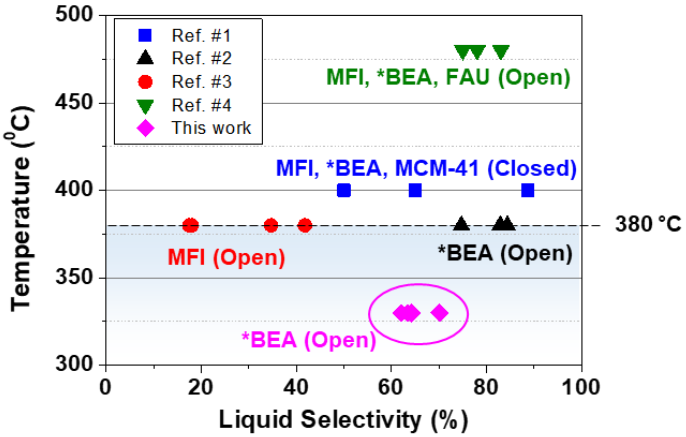


**Supplementary Figure 26. Schematic diagram comparing previous works and this study based on the liquid selectivity-temperature correlation: (**References: Ref #1: D. P. Serrano et al., *Ind. Eng. Chem. Res.* **39**, 1177–1184 (2000); Ref #2: V. P. S Caldeira et al., *Appl. Catal. A: Gen*. **531**, 187–196 (2017); Ref #3: A. Peral et al., *Catal. Sci. Technol.* **6**, 2754–2765 (2016); Ref #4: Y. Wang et al., *Catal. Today* **405**, 135–143 (2022).). Caldeira et al. focused on catalytic activity using hierarchical zeolite with enhanced mesoporous volume for accessibility to active sites. Extending this prior study, this work not only investigated the influence of process variables on catalytic cracking in an open-batch reactor but also examined the effects of the intrinsic properties of zeolites such as aluminum site density and crystal size.

Serrano et al. investigated the influence of zeolite pore size on catalytic cracking using a closed-batch reactor at 400 °C.[9] The results demonstrated that liquid selectivity varied significantly based on the pore size, with distinct outcomes observed for ZSM-5, zeolite beta, and MCM-41. Caldeira et al. and Peral et al. showed that catalytic activity depends on accessibility to active sites using hierarchical zeolites in an open-batch reactor at 380 °C.[10,11] Hierarchical *BEA and MFI, which have enhanced mesoporous volumes to access polyolefins, resulted in higher catalytic activity compared to conventional *BEA and MFI. Y. Wang et al. elucidated the structure-catalytic activity relationship of typical zeolites in an open-batch reactor at 480 °C.[12] The study concluded that the product

type of catalytic cracking was determined by the structure type of zeolites. The highest yield of gasoline components was achieved from zeolite beta, while aromatization products were obtained from zeolite Y and ZSM-5.

Previous open-batch studies have primarily focused on the impact of catalyst structures or properties on catalytic cracking. Extending this prior knowledge, our study experimentally demonstrated the influence of process variables on catalytic cracking within an open-batch reactor, highlighting their effects on conversion and liquid selectivity, suggesting the direction for the optimal catalyst and reactor configuration to achieve both high activity and high liquid selectivity.

## References


1 Jon, H., Lu, B., Oumi, Y., Itabashi, K. & Sano, T. Synthesis and thermal stability of beta zeolite using ammonium fluoride. *Microporous Mesoporous Mater.* **89**, 88-95 (2006).

2 Xie, B. *et al.* Organotemplate-Free and Fast Route for Synthesizing Beta Zeolite. *Chem. Mater.* **20**, 4533-4535 (2008).

3 Mintova, S. *et al.* Variation of the Si/Al ratio in nanosized zeolite Beta crystals. *Microporous Mesoporous Mater.* **90**, 237-245 (2006).

4 Munir, D., Amer, H., Aslam, R., Bououdina, M. & Usman, M. R. Composite zeolite beta catalysts for catalytic hydrocracking of plastic waste to liquid fuels. *Mater. Renew. Sustain. Energy.* **9**, 9 (2020).

5 Al-Khattaf, S. & de Lasa, H. The role of diffusion in alkyl-benzenes catalytic cracking. *Applied Catalysis A: General* **226**, 139-153 (2002).

6 Post, J. G. & van Hooff, J. H. C. Acidity and activity of H-ZSM—5 measured with NH3-t.p.d. and n-hexane cracking. *Zeolites* **4**, 9-14 (1984).

7 Vance, B. C., Kots, P. A., Wang, C., Granite, J. E. & Vlachos, D. G. Ni/SiO2 catalysts for polyolefin deconstruction via the divergent hydrogenolysis mechanism. *Appl. Catal. B* **322**, 122138 (2023).

8 Tamura, M. *et al.* Structure-activity relationship in hydrogenolysis of polyolefins over Ru/support catalysts. *Appl. Catal. B* **318**, 121870 (2022).

9 Serrano, D. P., Aguado, J. & Escola, J. M. Catalytic cracking of a polyolefin mixture over different acid solid catalysts. *Ind. Eng. Chem. Res.* **39**, 1177-1184 (2000).

10 Caldeira, V. P. *et al.* Properties of hierarchical Beta zeolites prepared from protozeolitic nanounits for the catalytic cracking of high density polyethylene. *Appl. Catal. A: Gen.* **531**, 187-196 (2017).

11 Peral, A. *et al.* Bidimensional ZSM-5 zeolites probed as catalysts for polyethylene cracking. *Catal. Sci. Technol* **6**, 2754-2765 (2016).

12 Wang, Y. *et al.* Elucidating the structure-performance relationship of typical commercial zeolites in catalytic cracking of low-density polyethylene. *Catal. Today* **405-406**, 135-143 (2022).